

Characterizing the Present-Day Activity of the Tunka and Sayan Faults Within Their Relay Zone (Western Baikal Rift System, Russia)

J.F. Ritz, A. Arzhannikov, R. Vassallo, S. Arzhannikov, C. Larroque, J.-L. Michelot, M. Massault

▶ **To cite this version:**

J.F. Ritz, A. Arzhannikov, R. Vassallo, S. Arzhannikov, C. Larroque, et al.. Characterizing the Present-Day Activity of the Tunka and Sayan Faults Within Their Relay Zone (Western Baikal Rift System, Russia). Tectonics, 2018, 37 (5), pp.1376-1392. 10.1002/2017TC004691 . hal-01851899

HAL Id: hal-01851899
https://hal.umontpellier.fr/hal-01851899

Submitted on 31 Jul 2018

HAL is a multi-disciplinary open access archive for the deposit and dissemination of scientific research documents, whether they are published or not. The documents may come from teaching and research institutions in France or abroad, or from public or private research centers.

L'archive ouverte pluridisciplinaire **HAL**, est destinée au dépôt et à la diffusion de documents scientifiques de niveau recherche, publiés ou non, émanant des établissements d'enseignement et de recherche français ou étrangers, des laboratoires publics ou privés.

AGU100 ADVANCING EARTH AND SPACE SCIENCE

Tectonics

RESEARCH ARTICLE
10.1002/2017TC004691

Key Points:
- Morphological investigations along the Sayan and Tunka faults at the southwestern tip of the Baikal rift show recent inversion of their vertical component
- The horizontal left-lateral slip rate along the Sayan-Tunka active faults system is estimated between 1.3 and 3.9~mm/year
- Paleoseismological investigations show that the eastern Sayan and Tunka faults produced Mw 7–8 earthquakes separated by ~4~kyrs recurrence intervals during the past 15~ka and that the two faults could have ruptured together or during seismic clusters

Supporting Information:
- Supporting Information S1

Correspondence to:
J.-F. Ritz,
jean-francois.ritz@gm.univ-montp2.fr

Citation:
Ritz, J.-F., Arzhannikova, A., Vassallo, R., Arzhannikov, S., Larroque, C., Michelot, J.-L., & Massault, M. (2018). Characterizing the present-day activity of the Tunka and Sayan faults within their relay zone (western Baikal rift system, Russia). *Tectonics*, *37*, 1376–1392. https://doi.org/10.1002/2017TC004691

Received 8 JUN 2017
Accepted 4 MAR 2018
Accepted article online 18 APR 2018
Published online 15 MAY 2018

©2018. American Geophysical Union. All Rights Reserved.

Characterizing the Present-Day Activity of the Tunka and Sayan Faults Within Their Relay Zone (Western Baikal Rift System, Russia)

J.-F. Ritz[1], A. Arzhannikova[2], R. Vassallo[3], S. Arzhannikov[2], C. Larroque[4], J.-L. Michelot[5], and M. Massault[5]

[1]Géosciences Montpellier, CNRS, Université de Montpellier, Montpellier, France, [2]Institute of the Earth Crust, Russian Academy of Sciences, Siberian Branch, Irkutsk, Russia, [3]Université Savoie Mont Blanc, Isterre, CNRS, Université Grenoble Alpes, IFFSTAR, Grenoble, France, [4]Géoazur, CNRS-IRD-OCA, Université de Nice Sophia Antipolis, Valbonne, France, [5]GEOPS, CNRS, University Paris-Sud, UMR 8148, Université Paris-Saclay, Orsay, France

Abstract The Sayan and Tunka faults are located at the boundary between the northernmost mountain belt of Central Asia (the Sayan-Baikal ranges) and the Siberian platform. These prominent crustal structures were involved in the opening of the southern Baikal rift system since the beginning of the Cenozoic and define large-scale sharp morphotectonic features. Despite low instrumental seismic activity, Late Pleistocene-Holocene morphotectonic features along the two faults indicate that the faults are active and have the capacity to produce strong earthquakes. A careful mapping of the most recent trace of activity, within the south-eastern parts of the two faults where they merge within a relay zone, demonstrates that they correspond now to left-lateral-reverse faults, suggesting a recent inversion of their vertical component. We also show that the two faults are now structurally connected via a young surface rupture and that no obvious post-Last Glacial Maximum ruptures are observed along the central part of the Sayan Fault beyond its junction zone with the Tunka fault. This suggests that the left-lateral strike-slip deformation is transferred from the eastern Sayan fault to the Tunka fault. A detailed morphotectonic study along the south-eastern Sayan fault allows estimating a left-lateral slip rate between 1.3 (min) and 3.9 mm/year (max). Finally, a critical review of Russian paleoseismic data, combined with our paleoseismological investigations, allows us to propose that the mean recurrence time along the two faults is on the order of 4 kyr and that they may have either ruptured together or during seismic clusters.

1. Introduction

The Sayan and Tunka faults are located at the boundary between the northernmost mountain belt of Central Asia (the Sayan-Baikal ranges) and the Siberian platform (e.g., Tapponnier & Molnar, 1979). These faults are several hundred kilometer long with sharp large-scale morphological traces (Figure 1). Usually, such morphotectonic features are characteristics of active faults (e.g., Baljinnyam et al., 1993; Berryman et al., 1992; Tapponnier & Molnar, 1977). The Sayan and Tunka faults display a microseismic activity, and a few paleoearthquake ruptures have been described notably at their junction zone (e.g., Chipizubov & Smekalin, 1999; Chipizubov et al., 2003; Ivanov et al., 2010) showing that these faults can produce strong earthquakes, like nearby faults within the south-Baikal rift system (e.g., Delouis et al., 2002; Déverchère et al., 2000; Sankov et al., 2004). They represent therefore potential strong seismic hazards for the city of Irkutsk and its suburbs (about 900,000 inhabitants) located 70 km to the north-east (station "IRKT" in Figure 1a). Nevertheless, both faults remain poorly described in terms of their present-day kinematics, their slip rate, and their earthquake potential.

In this paper, we present new morphotectonic and paleoseismic observations at the eastern parts of the Sayan and Tunka faults within their relay zone at the southwestern tip of the Baikal Lake. Our results allow characterizing the distribution and the kinematics of the most recent deformations. Combined with a synthesis of the main paleoseismological investigations carried out in the region, our observations also allow discussing the question of the seismic activity associated with the two faults.

2. Seismotectonic Setting

The Sayan fault extends several hundred kilometers northwestward from the Baikal Lake (Figure 1). This fault zone defines a major geological boundary between the Siberian platform to the north, and the orogenic

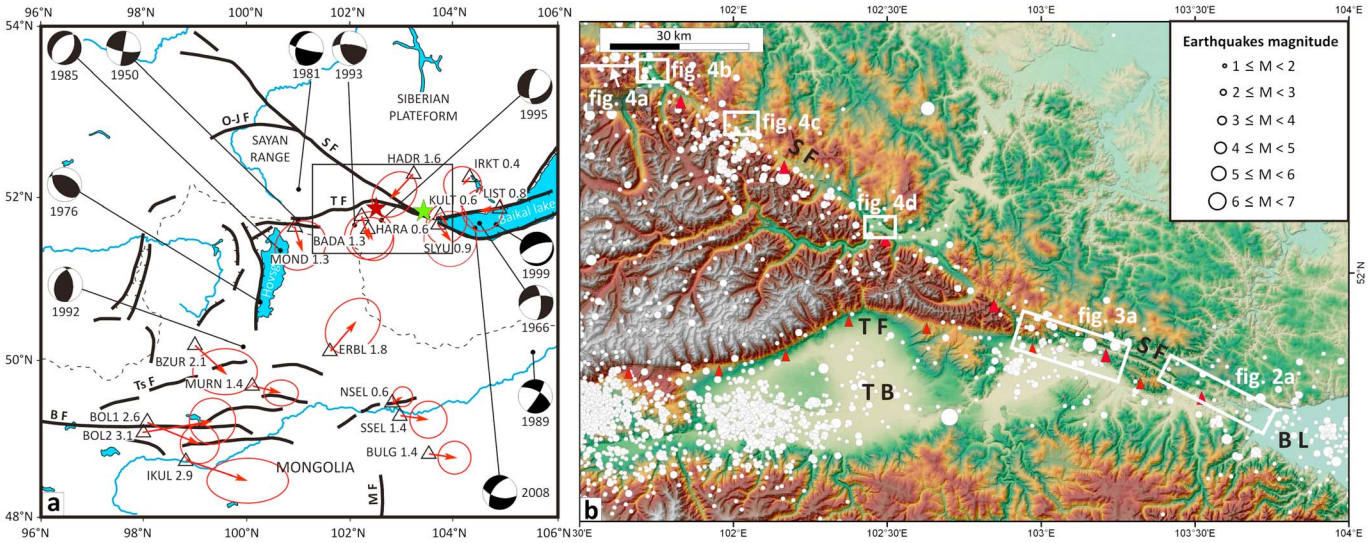


Figure 1. (a) Map of the main active faults (black lines) in northern Mongolia-southwestern Baikal region with focal mechanisms of M > 4.5 earthquakes and GPS velocities (mm/year) from Calais et al. (2006). The dashed black line shows the border between Mongolia and Russia; the blue lines are the main rivers. The green and red stars represent the locations for the 1742 and 1814 historical events, respectively, according to Chipizubov (2017), and Radziminovich and Shchetnikov (2016). Note, however, that these two locations bear wide uncertainties. (b): SRTM topomap of the Sayan and Tunka faults with seismicity (1960–1997 M ~ 2.2–6.3, catalog of the regional seismological network, Institute of the Earth Crust, Irkutsk). SF: Sayan fault, TF: Tunka fault, O-J F: Oka-Jombolok fault, BF: Bulnay fault, TB: Tunka basin, BL: Baikal Lake. The white frames locate Figures 2a, 3a, and 4a–4d.

domain of the Sayan-Baikal ranges to the south. The Siberian platform corresponds mainly to the Angara Archean craton (Melnikov et al., 1994) and has been poorly deformed since the Paleozoic (e.g Berzin, 1967; Zorin et al., 1993). The Sayan-Baikal orogenic belt results from Precambrian to Mesozoic subduction-collision processes between three domains: the Eurasia (Angara craton) to the north, the Mongolia-northern China block to the south, and the Mongol-Okhotsk Ocean to the east (Delvaux et al., 1995; Sengöret al., 1993; Zonenshain & Savostin, 1981; Zonenshain, Kusmin, & Natapov, 1990; Zorin et al., 1993; Zorin, 1999). The Sayan-Baikal orogenic belt is made of granitic, granodioritic, and ophiolic Precambrian terranes with volcano-sedimentary rocks of arc origin and Precambrian to Cenozoic ages (Melnikov et al., 1994).

During the beginning of the Cenozoic, the belt was affected by a large domal uplift associated with NW-SE extension that led to the opening of the Baikal basin and its south-westward associated basins (e.g., Logatchev, 1993). The origin of these large deformations is thought to be related to an asthenospheric diapirism process (e.g., Ermikov, 1994; Gao et al., 1994; Ionov, 2002; Logatchev & Zorin, 1992) and/or the far field effects of the India-Eurasia collision and/or the eastern Pacific subduction (e.g., Chemenda et al., 2002; Molnar & Tapponnier, 1975; Nataf et al., 1981; Tiberi et al., 2008). During this extensional tectonic phase, left-lateral strike-slip movement occurred along the Sayan fault allowing the opening of the Baikal rift (e.g., Lamakin, 1968; Logatchev, 1993; Misharina et al., 1983; Sherman et al., 1973; Sherman, 1978).

One of the associated basins that formed contemporaneously with the opening of the Baikal rift is the Tunka Basin, which defines a 200-km long and 30-km wide E-W depression at the southwestern extremity of the Baikal rift (Figure 1b). The Tunka basin corresponds to a northward tilted half-graben filled with Oligocene to Quaternary sediments (Logatchev & Zorin, 1987). To the north, the basin is clearly controlled by the Tunka fault, which defines typical facets spurs in the landscape (e.g., Larroque et al., 2001), with a 2-km difference in height between the crest of the Sayan Range and the basin surface. If the main normal component associated with the Neogene tectonics along the Tunka fault is obvious, its present kinematics is still under debate: some authors describe the fault as a normal-sinistral or pure normal fault (e.g., Lunina & Gladkov, 2004; McCalpin & Khromovskykh, 1995; Sherman, 1978); others mention reverse faulting along some parts of the eastern E-W trending section of the fault (e.g., Chipizubov et al., 2003; Ruzhich et al., 1972; Sankov et al., 1997).

Several works have pointed out a present-day transpressional tectonic to the west of the Baikal Lake in the transition area between the compressional tectonics in Central Mongolia and the extensional deformation in the central Baikal rift (Arjannikova et al., 2004; Arzhannikova et al., 2005, 2011; Delouis et al., 2002; Larroque et al., 2001; Parfeevets & Sankov, 2006; Sankov et al., 2004; Shchetnikov, 2016). These

Table 1
Focal Mechanisms of M > 4.5 Earthquakes in the Baikal-Mongolia Region

Date	Lat (°N)	Lon (°E)	M	Strike	Dip	Rake	Ref
4/4/1950	51.77	101.00	6.9	100	75	0	1
30/8/1966	51.36	100.61	5.0	25	48	102	1
1/4/1976	50.62	100.22	4.5	293	48	72	1
1/12/1981	52.18	101.00	5.0	203	40	−168	1
6/4/1985	51.36	100.61	4.8	25	48	−102	1
13/5/1989	50.17	105.34	5.7	31	82	−155	2
5/2/1992	50.16	99.97	5.6	206	42	116	1
13/1/1993	51.68	102.14	4.5	167	46	155	1
29/6/1995	51.71	102.70	5.8	84	44	−40	2
25/2/1999	51.64	104.82	6.0	249	70	−88	2
27/8/2008	51.60	104.04	6.3	104	63	−47	2

Note. Date, latitude, longitude, magnitude, strike and dip of the fault plane, rake of the slip vector, and reference: 1: Delouis et al., 2002; 2: Radziminovich et al., 2013).

observations concern mainly the region located at the westernmost part of the Tunka basin and its westward junction with the Hovsgol rift (i.e., the E-W trending Mondy valley; see station "MOND" in Figure 1a).

Several historical earthquakes occurred in the Tunka-Sayan area (Chipizubov, 2010; Kondorskaya & Shebalin, 1982; Shebalin & Leydecker, 1997). Nevertheless, as highlighted by Radziminovich and Shchetnikov (2013) and Tatevossian et al. (2013), many problems related to the reliability of data sources led to mistakes in the parametric catalogs. These authors concluded that the parameters of many known earthquakes in the eighteenth to nineteenth centuries in the Baikal region have to be refined. In Figure 1a, we only mention the 1742 Common Era (CE) and the 1814 CE events, which were recently reappraised. The macroseismic epicenter of the 27 June 1742 earthquake would be located at 51.8°N–103.4°E with an estimated magnitude between 7 and 8 (Chipizubov, 2017). After Chipizubov (2017), this historical event would be associated with the Sayan fault. The macroseismic epicenter of the 2 September 1814 (Gregorian calendar) earthquake would be located at 51.9°N–102.4°E with an estimated magnitude of 6.4 (Shebalin & Leydecker, 1997). This event is often attributed to a fault inside the Tunka basin (Radziminovich & Shchetnikov, 2013). However, the uncertainty on the macroseismic location being in the range of several tens of kilometers (Shebalin & Leydecker, 1997), it cannot be excluded that the eastern Tunka fault may not be the source of the 1814 historical event.

The instrumental seismicity recorded over the last 50 years by the regional network of the Institute of the Earth Crust in Irkutsk within the southwest Baikal rift region (e.g., Radziminovich et al., 2013) shows microseismic activity along the Sayan fault and within the Tunka basin (Figure 1b). The magnitudes of earthquakes are lower than Mw 5, with few events with magnitude close to 6 recorded in the Tunka basin and the southwestern Baikal Lake. The Sayan fault is characterized by an alignment of epicenters from the Baikal Lake to the SE until the junction with the Okino-Jombolok fault to the NW ("O-J F" in Figure 1a). The focal depths are between 5 and 50 km, as within the whole Baikal rift system region, which attests to the thickness of seismogenic crust (Déverchère et al., 1991).

From Baikal to Mongolia, the inversion of focal mechanisms (Delouis et al., 2002; Radziminovich et al., 2013) shows the variation of the deformation, from extension in the south Baikal area to compression in the Sayan area, while strike-slip deformation characterizes the southern Tunka and Mongolia regions. Focal mechanisms of M > 4.5 earthquakes point out the complexity of this deformation (Figure 1a and Table 1). In the Tunka basin, the stress tensor inversion from 18 focal mechanisms allowed Delouis et al. (2002) to determine a strike-slip stress regime with $\sigma 2$ close to vertical, while $\sigma 1$ and $\sigma 3$ are nearly horizontal with N212°E and N309°E directions, respectively. Earthquakes located at the southwestern end of the Baikal Lake suggest the continuation of the Sayan fault offshore with epicenters that are aligned along a NW-SE direction (Figure 1b). The Mw 6.3 Kultuk earthquake that occurred on 27 August 2008 in this area shows a left-lateral-normal faulting mechanism along a N104°E fault plane (Figure 1a), which is consistent with this interpretation.

Several papers analyzed the large-scale deformation of Asia including the Baikal area from Global Positioning System (GPS) measurements (Calais et al., 2003, 2006; Lukhnev et al., 2010; Vergnolle et al., 2003). Lukhnev et al. (2010) derived the strain pattern in the Baikal-Mongolia region from horizontal GPS velocities measured between 1994 and 2007. For the Hovsgol-Tunka-Sayan area, their study shows a transitional strain with a dominant shortening oriented N-S to NE-SW, while east of 104°E in the Baikal, the deformation is extensional with a stretching axis oriented NW-SE. These results are consistent with the stress analysis of Delouis et al. (2002) from focal mechanisms of earthquakes. At the longitude of 102°E, the ~5 mm/year displacement (eastwards component) between the north Chinese block and the Siberian platform is distributed along several major EW trending strike-slip faults: that is, the Bogd, Bulnay, Tunka, and the Sayan (Figure 1a). However, the lack of GPS stations near and on both sides of the Sayan and Tunka faults precludes determining precisely how much slip is accommodated along those faults. Sankov et al. (2004, 2014) stated that the present-day slip rate along the Sayan fault should be less than 3–5 mm/year. From GPS measurements (i.e., Calais et al., 2006; Lukhnev et al., 2010), the elastic left-lateral interseismic loading distributed between the Tunka and the Sayan

faults, northward the Bulnay fault, should be less than 2 mm/year. Paleoseismic investigations in the region suggest that five to six events would have occurred along the Sayan fault during the past 10 ka (Chipizubov & Smekalin, 1999; Sankov et al., 2004), while five events would have occurred along the Tunka fault during the past 11 ka (Chipizubov et al., 2003). These investigations also suggest that both faults are able to produce Mw7.3–Mw 8 earthquakes.

3. Analyzing the Present-Day Activity of the Tunka and Sayan Faults at Their Relay Zone

3.1. Distribution and Kinematics of the Most Recent Deformations

We used GoogleEarth and Bing satellites images to map carefully the scarps associated with the Sayan and the Tunka faults at their eastern termination (Figure 1b). Along the eastern Sayan fault (Figures 2a and S2 in the supporting information), the scarps define a N110°E trending almost-linear structure that crosses ridges, gullies, and basin catchments (Figures 2b–2d). These features show that the fault dip is close to the vertical. In a few places, we can observe displaced shutter ridges with horizontal offsets of several tens of meters attesting of the present main left-lateral movement along the fault (Figure 2c).

Along the easternmost part of the fault (Figure 2d), the scarps are distributed along two rupture lines showing different kinematics: along a northern line bending to the north, displacements appear mainly vertical and characterized by counterslope scarps affecting southward verging hillslopes (Figure 2e); along a southern N110°E trending line, at the base of the hillslope, aligned mole tracks indicate horizontal strike-slip displacement (Figure 2f). We interpret these features as the expression of a local surficial partitioning process of the deformation between steep reverse faulting along the northern surface rupture and left-lateral strike-slip faulting along the southern surface rupture.

Along the Tunka fault, clear fault scarps are found at the foothills of the Tunka ridge bounding the Tunka basin to the north (Figures 1 and 3). However, within the eastern part of the basin, the scarp line is clearly crossing through the alluvial plain associated with the Irkut River (Figures 3a and S3 in the supporting information). This feature suggests that the Irkut River has eroded part of the Tunka reliefs, but the fault remains active and affects alluvium. Three sites allow analyzing the kinematics of the fault:

1. At Bielly Camin, aligned mole-tracks define a linear surface rupture line located at the foothills of the mountain slope, without obvious vertical displacement from one side or the other (Figure 3b, left). About 1 km further east, the surface rupture defines a counterslope scarp cutting through two smooth interfluves (Figure 3b, right, and 3e). Here the fact that the apparent vertical component is larger eastward of the interfluves than westward attests of a left-lateral component (~8 m) in addition to the ~2 m uplift of the southward compartment.
2. Further east, 5 km northward of the village of Tory, the rupture defines also a counterslope scarp behind which a large sag pond has formed (Figure 3c). The pond is drained southward through a small channel incising the uplifted southern block. The morphology of the fault scarp and the structures affecting the fluvial material within a small trench, dug across the scarp, indicate that the ~2 m vertical uplift of the southern block is associated with reverse faulting (Figure 3f). Therefore, the features observed in Bielly Camin and Tory suggest that the normal component associated with the Tunka fault has been reversed very recently, during the Late Pleistocene-Holocene period.
3. About 10 km eastward the pond site, the fault seems to split into two branches: one scarp cuts through the Tunka ridge with a N070°E direction and connects with the Sayan fault zone (Figures 3a, 3d, and 3g). The formation of a lake due to the damming of the drainage suggests an uplift of the eastern block (i.e., the easternmost part of the Tunka ridge). The other scarp has a WNW-ESE direction following the foothills of the block and suggests also an uplift of the ridge (Figures 3g and S3 in the supporting information). We do not have field observations of these features; hence, we cannot conclude about their kinematics. However, taking into account that they correspond to the eastern extensions of the fault scarp observed within Tory, along which a clear reverse component is observed, we may assume that a reverse component is also present along the two fault scarps.

The fact that the present Tunka fault connects the Sayan fault raises the question of the transfer of the deformation between the two faults and also the question of the activity of the Sayan fault further to the NW, beyond the relay zone. To analyze whether the Sayan fault is still active nowadays within its central part,

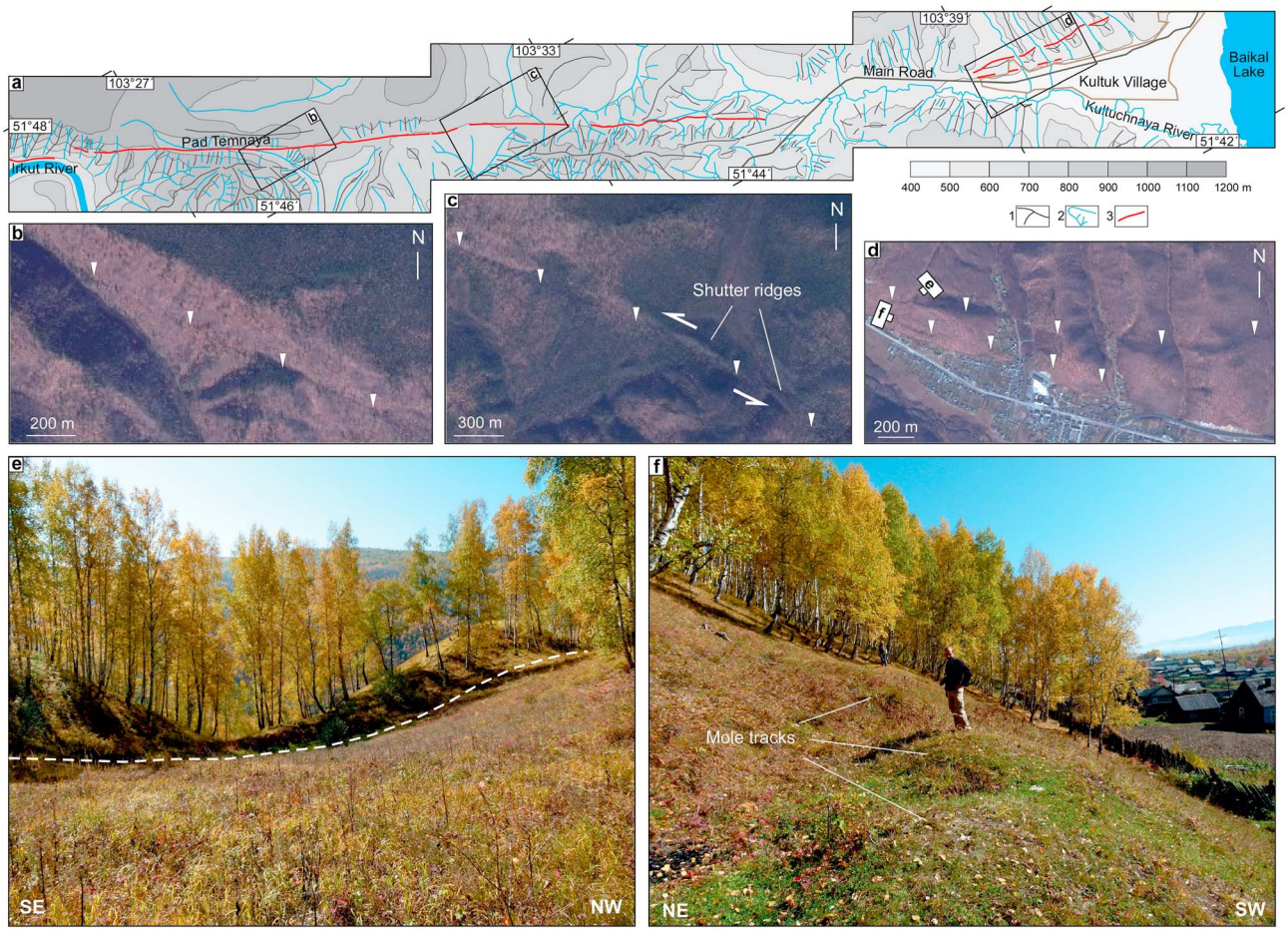


Figure 2. (a) Morphotectonic map interpreted from satellite images (see Figure S2 in supporting information) showing the drainage, the crest lines, and the fault lines in the morphology. (b) Bing satellite image seen in oblique view showing the Sayan fault scarp crossing in straight line through a basin catchment. (c) *idem* with evidences of left-laterally displaced shutter ridges. (d) Easternmost fault scarps associated with the Sayan fault showing the partitioning of the deformation between a steep dip-slip fault to the north (field picture e: 51°43.935′N, 103°38.970′E; the white dashed line follows the base of the fault scarp) and a linear sinistral strike-slip fault to the south (field picture f: 51°43.870′N, 103°38.890′E).

we used Bing and Digital Globe satellite images (with an estimated resolution of ~1 m per pixel), 12-m digital elevation models TanDEM-X, and 1/30,000-scale aerial photographs to map Last Glacial Maximum (LGM) and post-LGM morphotectonic features within sites where the drainage network is intersecting the Sayan fault (see Figure S4 in the supporting information). Figure 4 shows four sites studied in details where morphological features such as LGM moraines, kame terraces, and post-LGM geomorphic markers as fluvial terraces and terrace risers have been mapped.

Our analysis within the Dayalik river (Figure 4a), the Onot river (Figure 4b), the Malaya-Belaya river (Figure 4c), and the Kitoi river (Figure 4d) show that while the Sayan fault is clearly visible within the old markers in the landscape, no obvious deformation affects the LGM moraines and post-LGM fluvial markers (given the resolution of satellite images, we estimate that if a left-lateral offset was affecting these markers, it would be smaller than ~5 m (i.e., five pixels). This suggests that a large part, if not all, of the left-lateral deformation observed along the 70-km-long south-eastern part of the Sayan fault is transferred along the Tunka fault. Considering the age constrains for the LGM in the region (e.g., Arzhannikov et al., 2012, 2015), this suggests that the transfer is only 14–16 ka old.

Figure 5 summarizes our investigations in terms of distribution, geometry, and kinematics of active faulting along the eastern sections of the Sayan and the Tunka faults during the Holocene period. The two faults have a left-lateral kinematics with a reverse component, suggesting a recent inversion of their vertical component —at least along the Tunka fault where the long-term normal faulting is still well expressed in the large-scale



Figure 3. (a) Morphotectonic map interpreted from satellite images (see Figure S3 in the supporting information), same captions than Figure 2a. (b–d) Detailed views of Bing satellite images showing the fault scarps (white arrows). (e and f) Field pictures of the fault scarp in Bielly Camin (51°51.480′N, 102°59.000′E) and Tory (51°50.535′N, 103°4.580′E) sites, respectively. (g) Oblique NE view of a Bing satellite image showing the split of the Tunka fault rupture into two scarps lines around latitude 103°15′E (see location in Figures 3a and S3 in the supporting information).

topography. The Sayan and the Tunka faults appear now connected within a NE-SW trending fault. Further, the fact that we do not observe large cumulated deformations associated with these recent morphotectonic features suggests that this tectonic pattern emplaced recently, supposedly contemporaneously with the stop of the deformation along the central Sayan fault.

3.2. Estimating the Horizontal Slip Rate Along the Eastern Sayan Fault

Mapping morphotectonic features along the south-eastern section of the Sayan fault, we found out a small southward-oriented catchment basin affected by the fault where quaternary geomorphic markers and deposits could be used to estimate the horizontal slip rate along the fault (see Figure 5 for location). We surveyed the 50 × 400 m^2 area using an optical station and measured 2,430 topographic points from which we built up a digital elevation model (Figures 6 and 7a and Table S6 in the supporting information). The shaded relief in Figure 6 highlights a southwards scarp within the west-facing catchment slope (see field picture in Figure 7b) and a counterslope scarp within the east-facing catchment slope (see field picture in Figure 7c). These features attest of the main left-lateral horizontal movement along the Sayan fault. Note that the slightly southward arcuate shape of the scarp (Figure 6) indicates that the fault is dipping steeply toward the south.

To determine the cumulative left-lateral horizontal offset, we used the fact that there is no scarp in the topography along the fault between the coordinates 75 and 95 m, where the east-facing catchment slope becomes west facing (Figures 6 and 7a). This feature means that the slip vector is parallel to the topographic slope along the fault line (e.g., Nazari et al., 2009; Figure 8). We therefore determined the slip vector inclination (α) with respect to the horizontal by measuring the topographic slope between coordinates 75 and 95 m on the

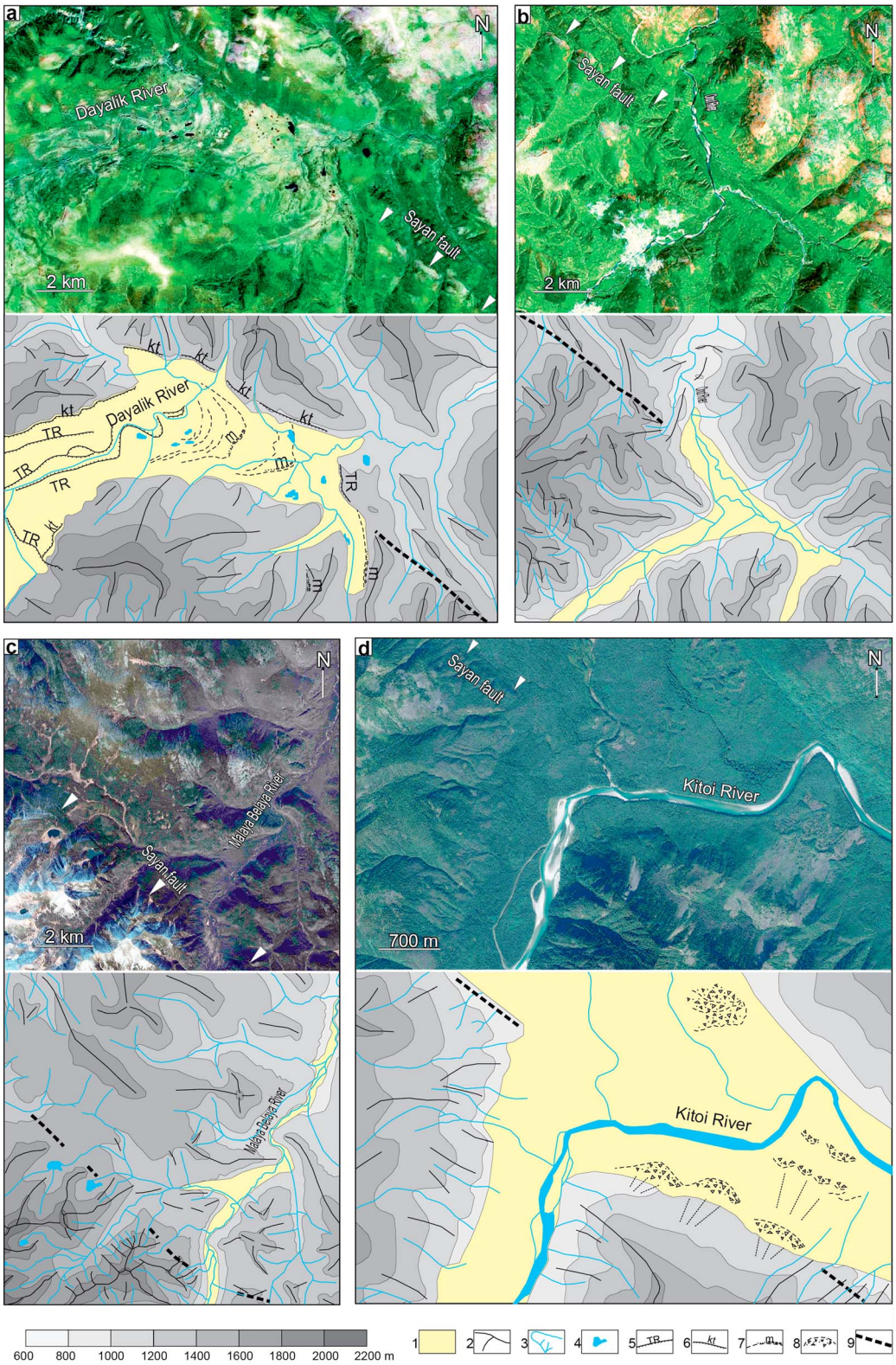


Figure 4. Satellite images of the four sites studied in details along the central part of the Sayan fault, and their corresponding morphological maps. (a) Dayalik river (center of the image: 52°28.340′N, 101°33.330′E). (b) Onot river (52°23.822′N, 101°43.718′E). (c) Malaya-Belaya river (52°10.531′N, 102°0.257′E). (d) Kitoi river (52°5.249′N, 102°27.480′E). 1: LGM and post-LGM deposits; 2: ridge and crests; 3: drainage; 4: lake; 5: terrace riser; 6: kame terrace; 7: moraine; 8: landslide; 9: Sayan fault (NB: no obvious LGM and post-LGM morphotectonics features were observed on 1/30,000-scale aerial photographs; we did not get authorization for their reproduction).

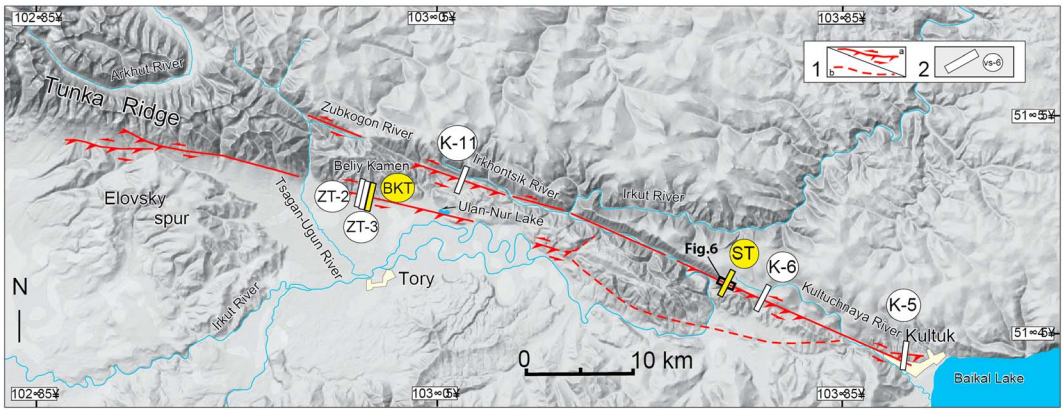


Figure 5. Synthetic sketch map of the present-day/Holocene deformations within the relay zone between Sayan and Tunka faults. 1: Faults and sense of motion (dashed fault lines indicate likely active features), the black frame indicates Figure 6 location (see section 3.2). 2: Trench sites and their names (the yellow circles are trenches analyzed during this study).

DEM. This yielded an inclination α of 13 ± 1° toward the west. Then, we estimated the cumulative vertical offset from topographic profiles across the fault scarp (Figure 7d). We obtained a mean value (*V*) of 8.6 ± 1.2 m. The horizontal offset (*H*) was eventually determined using the function $H = V/\tan(\alpha)$, which yielded a left-lateral cumulative offset of 37.5 ± 2.5 m. We obtained this same amount of horizontal offset when fitting piercing points (i.e., topographic features) from parallel profiles on both sides of the fault scarp (Figure 7e).

To estimate the age of formation of the scarp, we opened a trench (ST) in the sediments that were ponded against the north facing counterslope scarp in order to collect and date the first trapped deposits (Figures 6, 7a, and 7c for location; Figure 8). Figure 8d sketches the main units and the faulted zone (thick redline) that we observed in the 3-m-deep trench (depth at which we reached the permafrost). We distinguished four main detrital units that are affected by the fault in the lower part of the trench (units 60, 70, 80, and 100) and four units that are not affected in the upper part (units 50 to 20). The lithologic boundaries of the lower affected units (U60, U70, U80, and U100) are dipping southward. These deposits are bended against the fault zone suggesting that they have been deformed along the fault. The upper units (U50–U20) are dipping to the north. We interpret them as corresponding to scarp-derived colluvium associated with at least two surface-rupturing events (see next section).

We found few charcoals spread out in the different units allowing to constrain the age of the deposits (Table 2 and Figure 8d). Except two samples (SA11-13 and SA11-14), calibrated radiocarbon ages of samples are in stratigraphic order. Given the geometry of the trench with respect to the fault scarp (Figure 8c) and the change of size of the deposits at the bottom of the trench (i.e., fine deposits in unit 100 versus coarse deposits in unit 80; Figure 8e), we interpret unit 100 as corresponding to the colluvium covering the slope within the northern fault compartment (footwall) before the scarp formation. We therefore consider that sample (SA11-1), collected in unit 100, predates the scarp and represents therefore a

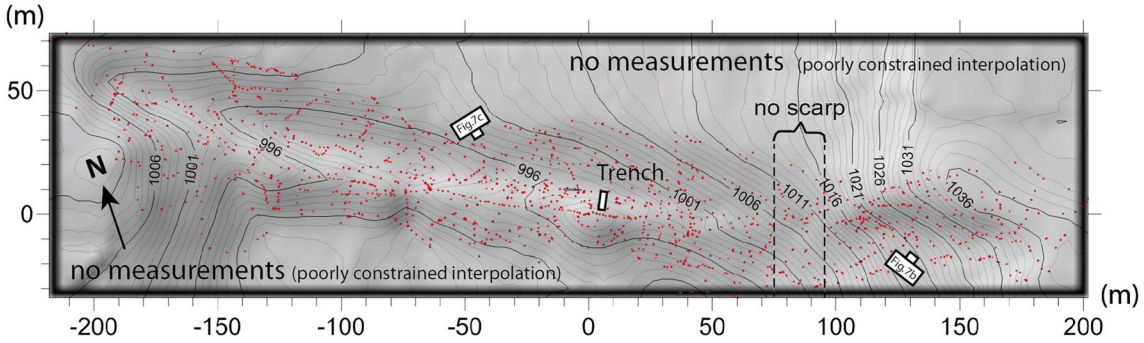


Figure 6. Shaded relief topographic map of the studied site along the Sayan fault for slip rate determination (see Figure 5 for location). The red dots correspond to the 2,430 topopoints from which was interpolated the topographic map using Surfer software and a Kriging gridding method. Note that indicated elevations (in meters) are approximate, N-S and E-W graduations also in meters.

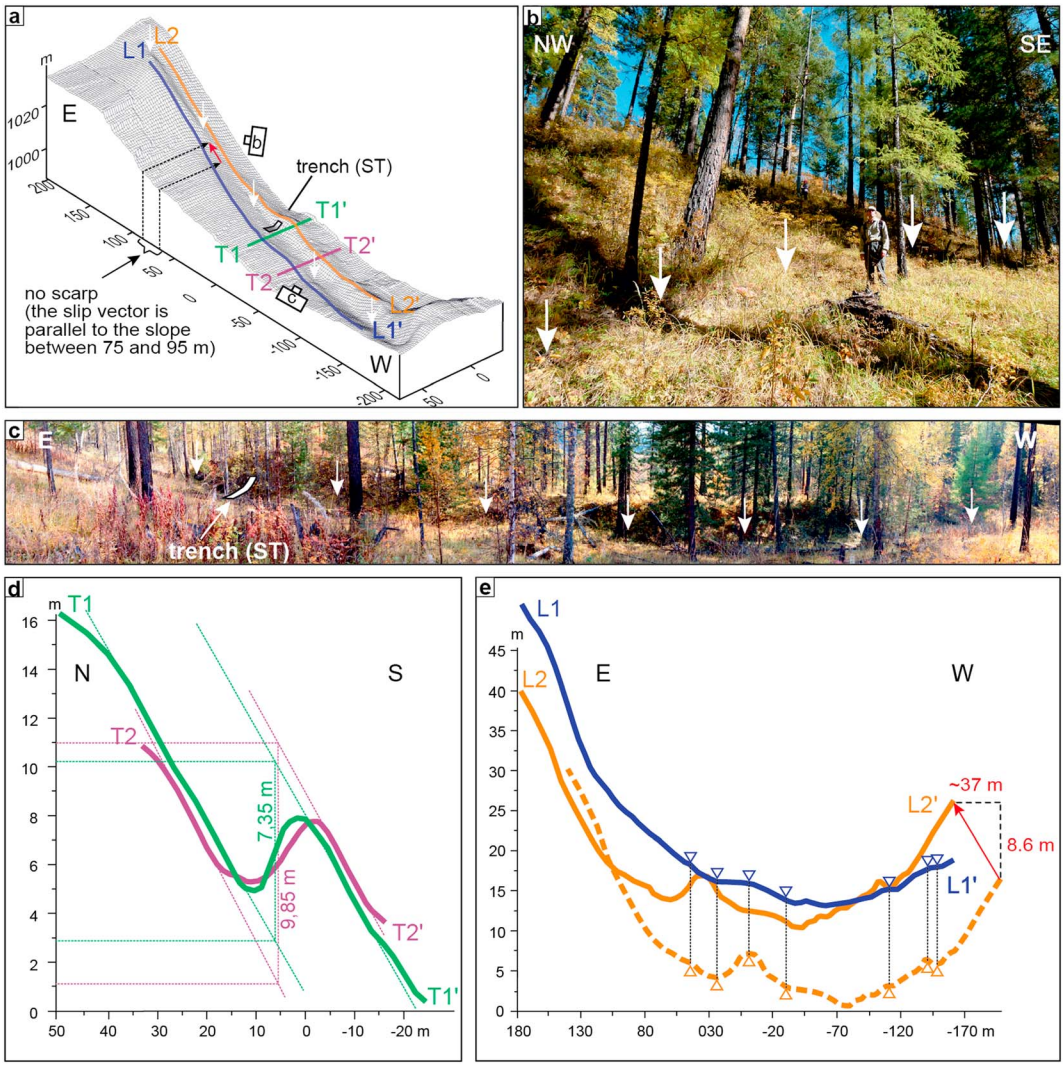


Figure 7. (a): 3-D view of the DEM of the studied site along the Sayan fault; the white arrows point out the base of the fault scarp (note that the slip vector [red arrow] is parallel to the topographic slope along the fault line between 75 and 95 m horizontal coordinates); L1 and L2 are parallel longitudinal profiles on both sides of the fault (L1 is located a few meters northward [upslope] the scarp to avoid the pond at the base of the scarp; L2 is located on top of the fault scarp); T1 and T2 are two cross profiles, locations, and orientation of the fault scarp pictures shown in b and c are indicated. (b) View of the fault scarp within its eastern part (scarp facing south, 51°47.195′N, 103°26.840′E). (c) Panoramic view of fault scarp (counterslope scarp facing north, 51°47.280′N, 103°26.660′E). (d) Cross profiles T1 and T2; (e) Longitudinal profiles L1 (blue line) and L2 (orange line); the blue and orange triangles point out piercing points (topographic features) between blue and dashed orange profiles before displacement; the red arrow shows the slip vector with its horizontal and vertical components (note that the two profiles mismatch vertically because they are not on the fault line).

maximum age for the scarp formation. Dividing the cumulative horizontal offset (37.5 ± 2.5 m) by the age of SA11-1 sample (27,340–27,710 calendar (cal) years before present [BP]) yields a minimum left-lateral slip rate along the Sayan fault of 1.4 ± 0.1 mm/year.

Conversely, the samples SA11-21a and 21b were collected into unit 80, which corresponds to trapped deposits (see Figures 8c and 8e). We therefore consider that they postdate the formation of the scarp. Dividing the cumulative horizontal offset by the age of SA11-21b (10,160–10,440 cal years BP) yields a maximum slip rate of 3.6 ± 0.3 mm/year. The left-lateral slip rate along the Sayan fault is therefore comprised between 1.3 and 3.9 mm/year.

3.3. Analyzing the Past Seismic Activity Along the Sayan and Tunka Faults Within Their Relay Zone

In order to analyze the seismic potential associated with the eastern Sayan and eastern Tunka faults, we analyzed the past seismic activity of the two faults within their relay zone. We compiled and synthetized the main

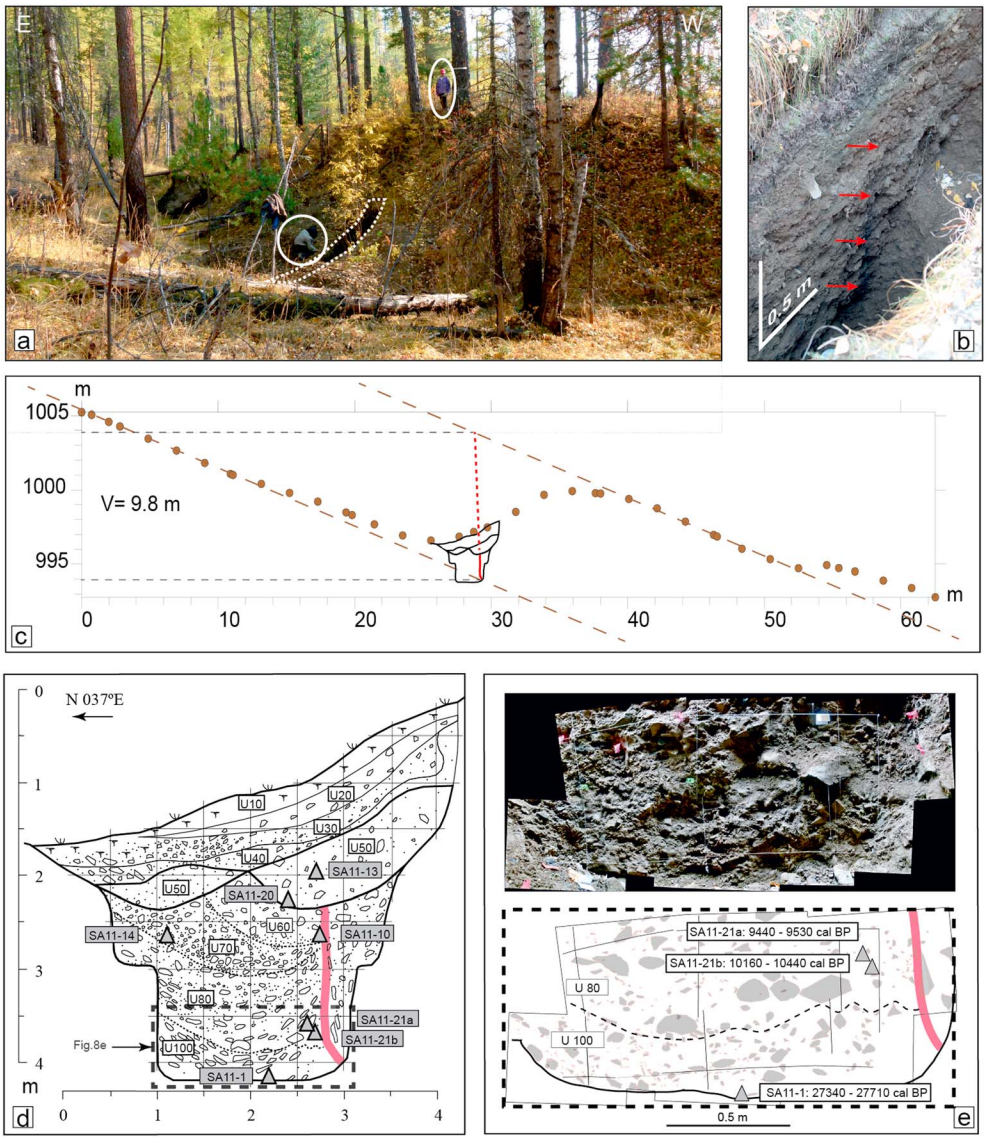


Figure 8. (a): Picture showing the counterslope scarp and the trench (white dashed line) opened in the trapped deposits (51°47.225′N, 103°26.755′E, circled peoples for scale). (b) Picture showing the fault zone sealed by unit (U50). (c) Geometry of the trench with respect to the scarp. (d) Log of the trench showing the main stratigraphic units, the faulted zone (redline), and collected samples. (e) Assembled photos and interpretation of the lower part of the trench (photomosaics of the trench walls were precluded given the trench narrowness).

Table 2
Calculated Dates From Radiocarbon Analysis of Charcoals Collected in Trench ST

Sample	Unit	^{14}C age year BP	±	Calibrated age, year BP (2σ)
SA11-1	U100	23,270	90	27,340–27,710
SA11-14	U70	29,030	140	32,840–33,640
SA11-13	U50	5,090	40	5,740–5,920
SA11-10	U60	8,720	40	9,550–9,820
SA11-20	U50	4,805	30	5,470–5,600
SA11-21a	U80	8,465	40	9,440–9,530
SA11-21d	U80	9,100	70	10,160–10,440

Note. Dendrochronologically calibrated calendar age ranges were calculated using the program Calib Radiocarbon Calibration (Stuiver et al., 2018) with 2 standard deviations uncertainty. The age ranges are rounded off to the nearest decade.

paleoseismological results published in Chipizubov and Smekalin (1999), Chipizubov et al. (2003), and Smekalin (2008), which we reinterpreted together with our data. Figure 9 presents trench-logs for which there is clear evidence of event horizons (i.e., ancient ground surface(s) affected by surface ruptures; e.g., McCalpin, 1996) with age constraints (Tables 2 and 3). Seven trenches are presented from the east to the west: K-5, K-6, ST, and K-11 for the Sayan fault (note that trench ST has already been described in section 3.2) and BKT, ZT-3, and ZT-2 for the Tunka fault (see Figure 5 for location).

As concerns the paleoseismological investigations along the eastern part of the Sayan fault, the main observations are as follows:

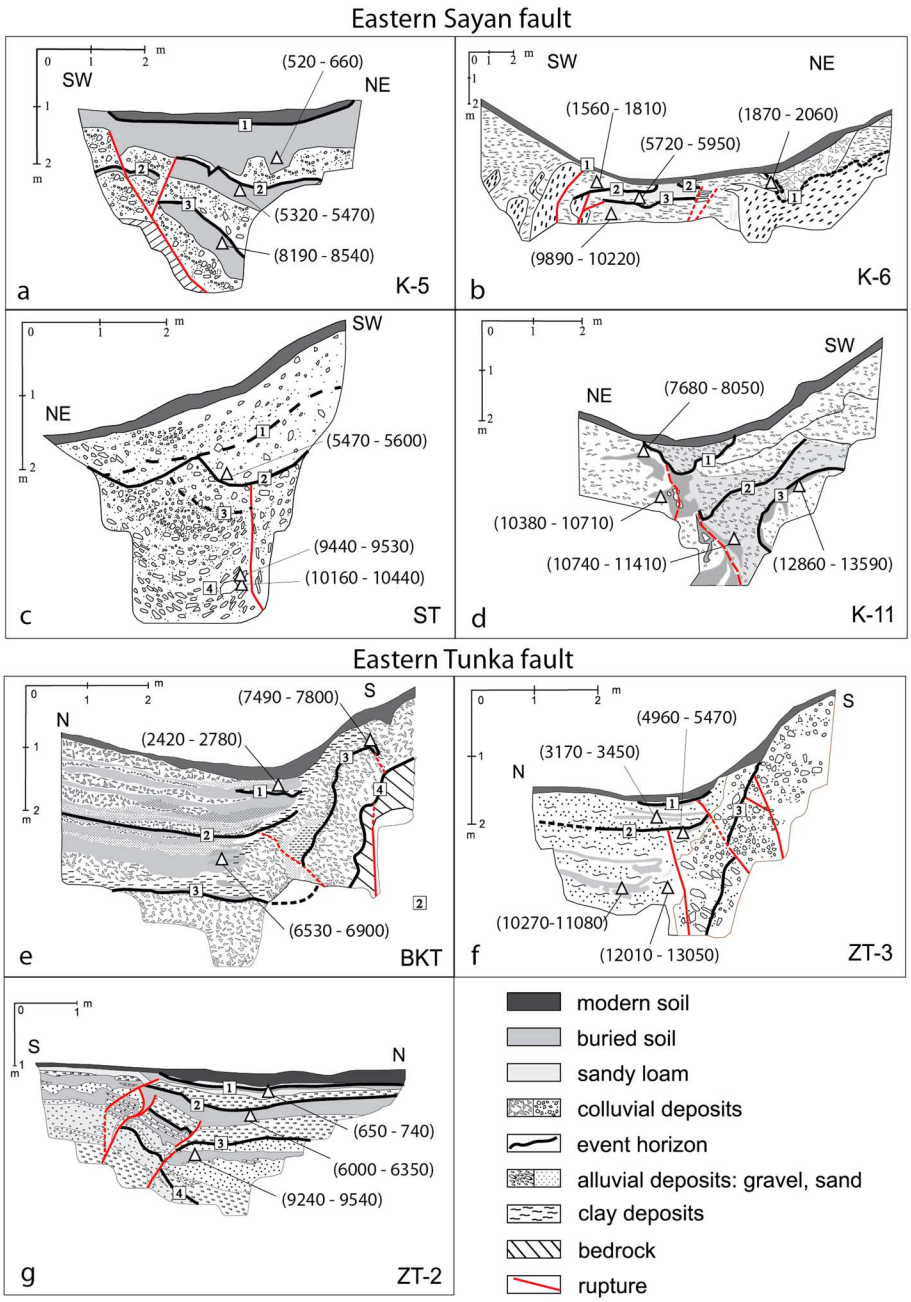


Figure 9. Synthetic logs of the seven studied trenches across the eastern Sayan and Tunka faults showing the event horizons (numbers are successive event horizons) and their age constraints (Figure 5 for location). K5, K6, K11, ZT3, and ZT2 logs were reproduced as they are in Chipizubov and Smekalin (1999) and Chipizubov et al. (2003). More details about these logs are given in Smekalin (2008).

In trench K5 (Figure 9a), three events can be interpreted from both fault termination criteria and stratigraphic evidence (i.e., faulted buried soil horizons). Radiocarbon dating of organic-rich material allows constraining a first event (the most recent) after 660 cal years BP, and a second event (the penultimate) between 520 and 5470 cal years BP. A third event bracketed between 5,320 and 8,540 cal years BP can be interpreted from a buried soil horizon that is faulted and buried below a colluvium unit, itself overlain by the faulted and buried soil horizon defining the second event. Although there are no fault termination criteria allowing to clearly individualize this third event, this old faulted buried soil was considered as an event horizon given that it is not observed in the southwestern part of the trench below

Table 3
Calculated Calibrated Dates From Radiocarbon Analyses

Fault	Trench	Sample	^{14}C age year BP	±	Calibrated age, year BP (2σ)
Sayan fault	K-5	LU-2997*	580	60	520–660
		LU-2998*	4,670	30	5,320–5,470
		LU-2999*	7,570	90	8,190–8,540
	K-6	LU-3026*	1,760	50	1,560–1,810
		LU-3027*	2,000	40	1,870–2,060
		LU-3029*	5,110	60	5,720–5,950
		LU-3025*	8,920	60	9,890–10,220
	K-11	LU-3045*	7,070	100	7,680–8,050
		LU-3044*	9,340	60	10,380–10,710
		LU-3043*	9,760	110	10,740–11,410
		LU-3004*	11,420	180	12,860–13,590
Tunka fault	ZT-3	GIN-9604**	3,110	60	3,170–3,450
		GIN-9603**	4,550	90	4,960–5,470
		GIN-9602**	9,390	110	10,270–11,080
		GIN-9601**	10,700	210	12,010–13,050
	ZT-2	GIN-9600**	750	40	650–740
		GIN-9599**	5,440	70	6,000–6,350
		GIN-9598**	8,400	80	9,240–9,540
	BKT	H2660***	2,562	72	2,420–2,780
		H2661***	5,898	73	6,530–6,900
		H2662***	5,982	69	6,660–6,990
		H2659***	6,790	84	7,490–7,800

Note. Dendrochronologically calibrated calendar age ranges were calculated using the program Calib Radiocarbon Calibration (Stuiver et al., 2018) with 2 standard deviations uncertainty. The age ranges are rounded off to the nearest decade. (*), (**), (***): Data from Chipizubov and Smekalin (1999), Chipizubov et al. (2003), and this work, respectively.

the second event horizon. Moreover, the occurrence of an event in this time range is also suggested in the three other trenches (see below).

In trench K6 (Figure 9b), with the same kind of paleoseismic evidences, three events can be interpreted as well: the younger one occurred after 1,810 cal years BP, while the second and third events are bracketed between 1,560 and 5,950 cal years BP, and 5,720 and 10,220 cal years BP, respectively.

In trench ST (Figure 9c)—the trench that we dug to date the cumulative fault scarp presented in Figures 7 and 8—we identified at least three events: The two younger events occurred after 5,600 cal years BP, which corresponds to the age obtained for a charcoal collected at the base of the colluvial wedge unit U50 described in Figure 8d (*NB*: a colluvial wedge unit is postdating an event, but because it is scarped-derived, its constitutive detrital material such as clasts or charcoals predates the event). The third event occurred between 5,470 and 9,530 cal years BP. A fourth event occurred before 10,160 cal year s BP.

In trench K-11 (Figure 9d), a minimum of three events occurred in the past 13,600 years. They are materialized mainly by stratigraphic evidences (i.e., colluvium units sealing faulted structures). The younger event observed in the trench occurred after 8,050 cal years BP. Two older events are bracketed between 7,680 and 11,410 cal years BP, and between 10,740 and 13,590 cal years BP, respectively.

As concerns the paleoseismological investigations along the eastern part of the Tunka fault, the main observations are as follows:

In trench BKT (Figure 9e) we identified four events: We interpreted the small colluvial wedge unit interstratified with ponded sediments in the upper part of the trench, as corresponding to the most recent event (although we did not observe rupture criterion associated with it). Using the same interpretation of charcoal reworking than in trench ST along the Sayan fault (see above), we interpreted this event to be post 2,780 cal years BP. The second event is also defined by a colluvial wedge unit associated with an uncertain rupture criterion. Radiocarbon ages suggest that it occurred between 2,420 and 6,900 cal years BP. Two older events are materialized by thick colluvial wedges (with clear rupture terminations) and occurred before 7,490 cal years BP (age of trapped organic-rich material interstratified with the colluvial wedge deposits postdating the third event).

In trench ZT-3 (Figure 9f), located few hundred meters to the west from our trench BKT, Smekalin (2008) identified three events based on colluvial wedge occurrences and fault termination criteria. From radiocarbon ages, the first observed event occurred after 3,450 cal years BP. A second event occurred between 3,170 and 5,470 cal years BP, while an older event occurred before 12,010 cal years BP. Note that these data suggest a fairly long gap between the second and the third events. This is not consistent with our observations made within the nearby BKT trench and suggests that an event may have been missed.

In trench ZT-2 (Figure 9g), located slightly to the west from trench ZT-3, four events can be interpreted from Smekalin (2008) trench log: a fault termination criterion allows identifying a younger event (the most recent) that occurred after 740 cal years BP. A second event (the penultimate) occurred between 650 and 6,350 cal years BP. A third event occurred between 6,000 and 9,540 cal years BP. A fourth older event, materialized by an alluvial unit eroding and laying unconformably above a colluvium unit, occurred before 9,240 cal years BP.

Figure 10 shows the age constraints for the events interpreted from the four trenches presented for the eastern Sayan fault and the three trenches presented for the eastern Tunka fault. Combining the results for each fault allows tightening the timing of the latest events that occurred along them.

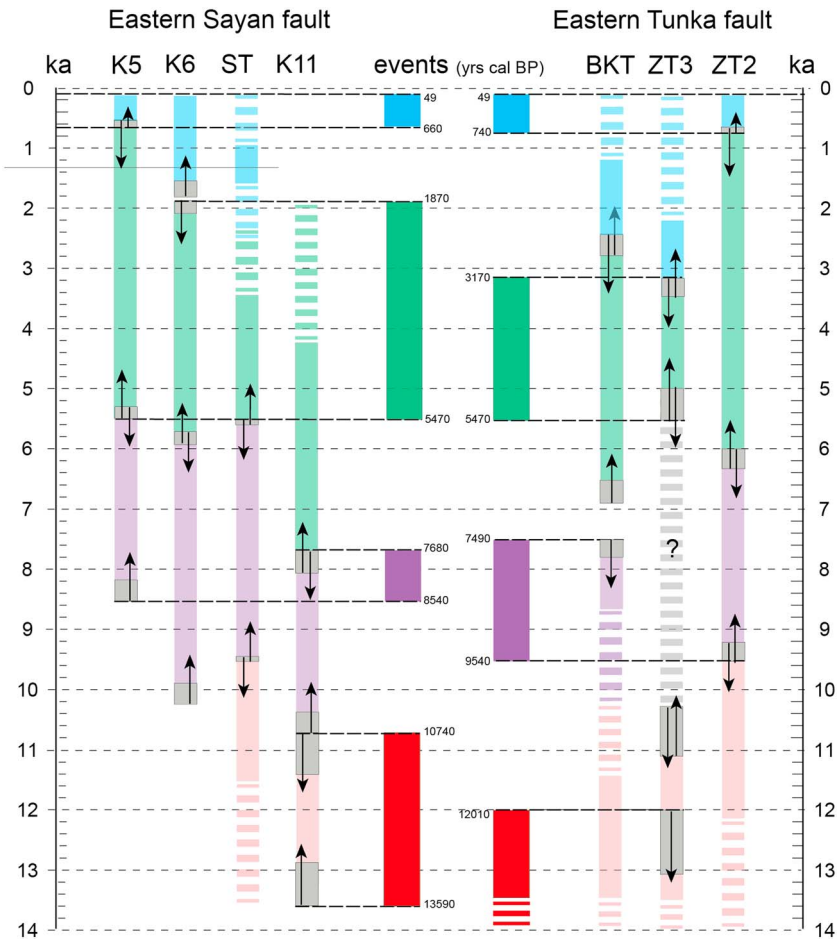


Figure 10. Sketch synthetizing the age constraints for the four past earthquakes observed in trenches K-5, K-6, ST, and K-11 along the Sayan fault and trenches BKT, ZT-3, and ZT-2 along the Tunka fault. The grey boxes correspond to calibrated ages, and the black arrows indicate the predating or postdating of the events. The light blue, green, purple, and pink colors define the time ranges during which the most recent, the penultimate, the prepenultimate, and the pre-pre-penultimate events occurred, respectively. The two central columns with denser colors combine the age constraints for each fault.

Along the eastern Sayan fault, the most recent event (1) has occurred between 1901 CE (i.e., 49 years before 1950 when referring to calibrated radiocarbon ages) and 660 cal years BP. The date of 1901 corresponds to the installation of the first "Irkutsk" seismological station and can be considered as the upper limit of the historical period (Radziminovich & Shchetnikov, 2013). Therefore, it is possible that the paleoseismic feature characterizing the first event in trench K5 (Chipizubov & Smekalin, 1999, our Figure 9a) corresponds to the 27 June 1742 historical event. The penultimate event (2), prepenultimate (3), and fourth (4) events would have occurred between 1,870 and 5,470, 7,680 and 8,540, and 10,740 and 13,590 cal years BP, respectively.

Along the eastern Tunka fault, the most recent event (1) would have occurred between 1901 CE and 740 cal years BP. Although there is no consensus on the precise location of the historical earthquakes in the Tunka region, the recent reappraisal of the 1814 CE earthquake by Radziminovich and Shchetnikov (2013) suggests that this event could be associated to the eastern Tunka fault. Therefore, the paleoseismic observations, notably in trench ZT2 (Chipizubov et al., 2003; Smekalin, 2008, our Figure 9g), could correspond to the 22 August 1814 historical earthquake. The penultimate event (2) and prepenultimate (3) would have occurred between 3,170 and 5,470, and 7,490 and 9,540 cal years BP, respectively. A fourth event occurred before 12,010 cal years BP. When comparing the temporal distribution of large events between the two faults (Figure 10), we note that they are overlapping. Both faults ruptured 4 times during the past 15 ka and show the same mean ~4 kyr return period for surface-rupturing earthquakes (i.e., 4.2 ± 0.3 kyr for Sayan and 3.9 ± 0.6 kyr for Tunka). This distribution of events suggests that the two faults may have ruptured together or during clustered events.

4. Discussion

The careful mapping of the fault scarps along the Sayan and Tunka faults within their relay zone allows showing that the two faults have a left-lateral kinematics with a reverse component. This suggests a recent inversion of their vertical component, from normal to reverse, notably along the eastern Tunka fault. This is consistent with our previous morphotectonic studies within the western part of the Tunka basin (Arjannikova et al., 2004; Larroque et al., 2001; Ritz et al., 2000) as well as the observations published in Chipizubov et al. (2003) about the central and eastern parts of the Tunka fault, and Chipizubov and Smekalin (1999) and Sankov et al. (2004) about the eastern part of the Sayan fault. The analysis of the most recent morphotectonic features suggests that the Sayan and the Tunka faults are now connected within a NE-SW trending fault. The careful analysis of satellites images and aerial photographs show that no obvious deformations are observed within the post-LGM geomorphic markers along the Central Sayan fault, beyond the 70 km long south-eastern section. We may wonder whether this section of the fault could have stayed quiescent, without producing large surface-rupturing events during a period of 14–16 kyr. However, considering our slip rate estimate (1.3–3.9 mm/year), this would represent a slip deficit comprised between 24 and 62 m. It seems therefore difficult to consider that the Central Sayan fault is still producing large earthquakes (at least regularly) and suggests that a large part, if not all, of the left-lateral strike-slip deformation observed along its eastern part is transferred along the Tunka fault since the past ~15 ka.

The 1.3–3.9 mm/year left-lateral slip rate estimated along the Sayan-Tunka fault system, together with the slip rates estimated along the Bogd fault and the Bulnay fault in Mongolia (i.e., ~1 and ~2.5 mm/year, respectively; Ritz et al., 1995, 2006; Rizza et al., 2011, 2015), is consistent with the ~5 mm/year eastward component of displacement of the north Chinese block relatively to the Siberian platform (Calais et al., 2003).

Our synthesis of the main paleoseismic observations made along the eastern Sayan and eastern Tunka faults shows that four events occurred within the past 15 ka along the two faults with a mean return period of 3.9–4.2 ka for both faults. Our interpretations differ with previous ones: Chipizubov and Smekalin's (1999) study, reinterpreted in Sankov et al. (2004), concluded that five events had occurred along the eastern Sayan fault during the past 10 ka, with the following bracketed ages: ~400–1,100 (1), ~1,800–2,600 (2), 4,200–5,100 (3), 7,000–7,700 (4), and 8,400–9,700 (5) years BP. Along the Tunka fault, Chipizubov et al. (2003) concluded that six events had occurred during the past 11 ka, with the following bracketed ages: 1,315–1,742 (1), 2,464–2,809 (2), 5,227–5,907 (3), 7,091–7,385 (4), 9,214–9,902 (5), and 10,386–11,187 (6). These results suggest smaller recurrence intervals (i.e., ~2,000 years) for earthquakes, along both faults. Although some of these results are consistent with ours—it is the case, for instance, for the third and fourth events on both faults—we think that paleoseismic features presented in the above-mentioned works have been incorrectly interpreted and/or overinterpreted.

Multiplying the lower and maximum bounds of the slip rate (i.e., 1.3 and 3.9 mm/year) by the mean recurrence time yields an average horizontal slip per event comprised between 5 and 16 m. When compared with Chipizubov and Smekalin's (1999) slip observations along the Sayan fault (i.e., 4–10 m of horizontal slip for a single event) and Chipizubov et al.'s (2003) observations along the eastern Tunka fault (i.e., 3.5–8 m of horizontal slip for a single event), this suggests that the slip rate of the Sayan-Tunka fault system within its relay zone is closer to the lower bound.

The distribution through time of events along the two faults suggests that they can rupture contemporaneously during strong events, or successively during earthquakes clustering. This is supported by the paleoseismic records. For instance, the third event along both faults occurred in the time range of 7.5–9.5 ka and is materialized by thick scarp-derived colluvium (it is particularly clear along the Tunka fault; see Figures 9e and 9f). This is also the case for the fourth event. This shows that the corresponding scarps were big and were probably produced by large surface rupturing events.

This interpretation is consistent with offsets equal to or larger than 4 and 3.5 m that were estimated for strike-slip events along the Sayan and the Tunka faults, respectively (Chipizubov et al., 2003; Chipizubov & Smekalin, 1999). After statistical functions (e.g., Wells & Coppersmith, 1994), these offsets correspond to earthquakes with moment magnitudes $Mw \geq 7.5$ that are associated with surface rupture length of at least 100 km. This suggests that large events would break both the 70-km-long active section of the eastern Sayan fault and a part of the Tunka fault.

Conversely, the stratigraphic signature for the two more recent events, with thinner scarp derived-colluvium units (Figures 9a, 9e, 9f, and 9g), suggests smaller surface rupturing events, and therefore independent ruptures between the two faults. However, the similar time ranges between events from a fault to another suggest that they could form a clustered sequence.

5. Conclusions

Our study brings new insights on the present-day kinematics, the slip rate, and the earthquake potential of the Tunka and Sayan faults within their relay zone:

The careful mapping of the most recent traces of activity, using Google Earth and Bing satellites images within the south-eastern parts of the two faults, shows that at present, the two faults are left-lateral strike-slip faults with a reverse component and are spatially connected. This confirms the establishment of a new tectonic regime within the southwestern edge of the Siberian platform during the Quaternary period.

Along the Central Sayan fault, beyond the 70-km long south-eastern section, our morphotectonic analysis including also aerial photographs shows that no obvious deformations are observed within the post-LGM geomorphic markers. This suggests that a large part of the left-lateral movement observed along the eastern Sayan fault seems now to be transferred along the Tunka fault, involving a diminution, if not an interruption of the activity along the central part of Sayan fault.

The detailed morphotectonic study of a fault scarp along the south-eastern Sayan fault (building up a digital elevation model with a total station for determining the cumulative horizontal offset and opening a trench for dating the trapped sediments) allows bracketing the left-lateral slip rate along the fault between 1.3 and 3.9 mm/year.

The compilation and reinterpretation of the main paleoseismological results published in Russian literature along with our own paleoseismological investigations show that the eastern Sayan and Tunka faults have produced magnitude Mw 7–8 earthquakes separated by mean recurrence periods of ~4 kyr during the past 15 ka. The similar time ranges between events from a fault to another suggest that they may have ruptured together or during clustered sequences. The 1745 CE and 1814 CE historical events, if they occurred on Sayan and Tunka fault respectively, could represent such a sequence.

Acknowledgments
This work gathers field observations made in 1999–2000 and 2011, carried out in the framework of a CNRS-INSU project and a French–Russian program for international scientific cooperation/Russian Fund for Basic Research (projects PICS 13-05-91052-CNRS-4881 and 17-55-150002). All data used in this study can be found in the tables and figures presented in the article and in its supporting information (i.e., topographic data used for building up the DEM presented in Figure 6). Remote sensing analyzing of morphotectonic features was done, thanks to the TanDEM-X project DEM_GEOL1193. We thank M. Jolivet, the coordinator of the PICS project on the French side for his support. Note that part of the radiocarbon samples were analyzed through Artemis-CNRS-INSU program and were prepared at GEOPS lab in Orsay by M. Massault. We thank V. Sankov, M. Lebedeva, A. Parfeevets, A. Chipizubov, O. Smekalin, J-F. Stéphan, P. Antoine, and M. Ferry for fruitful discussions. We also thank two anonymous reviewers and Laura Gregory for their thorough reviews, Pavel Smal for his help in translating Russian colleagues' works, and Taylor Schildgen and Guila Ganem for a final reading and editing of the manuscript.

References

Arjannikova, A., Larroque, C., Ritz, J.-F., Déverchère, J., Stéphan, J. F., Arjannikov, S., & Sankov, V. (2004). Geometry and kinematics of recent deformation in the Mondy–Tunka area (south-westernmost Baikal rift zone, Mongolia–Siberia). *Terra Nova*, *16*(5), 265–272. https://doi.org/10.1111/j.1365-3121.2004.00565.x

Arzhannikov, S., Braucher, R., Jolivet, M., & Arzhannikova, A. (2015). Late Pleistocene glaciations in southern East Sayan and detection of MIS 2 terminal moraines based on beryllium (10Be) dating of glacier complexes. *Russian Geology and Geophysics*, *56*(11), 1509–1521. https://doi.org/10.1016/j.rgg.2015.10.001

Arzhannikov, S., Braucher, R., Jolivet, M., Arzhannikova, A., Vassallo, R., Chauvet, A., et al. (2012). History of late Pleistocene glaciations in the central Sayan-Tuva Upland (southern Siberia)//Quaternary. *Science Reviews*, *49*, 16–32. https://doi.org/10.1016/j.quascirev.2012.06.005

Arzhannikova, A., Arzhannikov, S., Jolivet, M., Vassallo, R., & Chauvet, A. (2011). Pliocene to Quaternary deformation in South East Sayan (Siberia): Initiation of the Tertiary compressive phase in the southern termination of the Baikal rift system. *Journal of Asian Earth Sciences*, *40*(2), 581–594. https://doi.org/10.1016/j.jseaes.2010.10.011

Arzhannikova, A. V., Arzhannikov, S. G., Semenov, R. M., & Chipizubov, A. V. (2005). Morphotectonics and Late Pleistocene–Holocene deformations in the Tunka system of basins (Baikal rift, Siberia). *Zeitschrift für Geomorphologie*, *49*, 485–494.

Baljinnyam, I., Bayasgalan, A., Borisov, A., Cisternas, A., Dem'yanivitch, M., Ganbaatar, L., et al. (1993). Ruptures of major earthquakes and active deformation in Mongolia and its surroundings. *Geological Society of America Memoirs*, *181*, 62. https://doi.org/10.1130/MEM181-p1

Berryman, K. R., Beanland, S., Cooper, A., Cutten, H., Norris, R., & Wood, P. (1992). The Alpine fault, New Zealand: Variation in Quaternary structural style and geomorphic expression. *Annales Tectonicae*, *6*, 126–163.

Berzin, N. A. (1967). *The Main Sayan Fault in East Sayan* (in Russian) (147 pp). Nauka, Moscow.

Calais, E., Dong, L., Wang, M., Shen, Z., & Vergnolle, M. (2006). Continental deformation in Asia from a combined GPS solution. *Geophysical Research Letters*, *33*, L24319. https://doi.org/10.1029/2006GL028433

Calais, E., Vergnolle, M., Sankov, V., Lukhnev, A., Miroshnitenko, A., Amarjargal, S., & Déverchère, J. (2003). GPS measurements of crustal deformation in the Baikal-Mongolia area (1994–2002): Implications for current kinematics of Asia. *Journal of Geophysical Research*, *108*(B10), 2501. https://doi.org/10.1029/2002JB002373

Chemenda, A., Déverchère, J., & Calais, E. (2002). Three-dimensional laboratory modelling of rifting : Application to the Baikal rift, Russia. *Tectonophysics*, *156*, 253–273.

Chipizubov, A. V. (2010). Strong earthquakes in the Pribaikalie: Macroseismic data. *Seismic Instruments*, *46*(2), 177–192. https://doi.org/10.3103/S0747923910020064

Chipizubov, A. V. (2017). Problematic historical earthquakes in the Baikal region. *Seismic Instruments*, *53*(2), 155–172. https://doi.org/10.3103/S0747923917020062

Chipizubov, A. V., & Smekalin, O. P. (1999). Fault scarps and the causative prehistoric earthquakes in the main Sayan fault zone. *Russian Geology and Geophysics*, *40*(6), 921–931.
Chipizubov, A. V., Smekalin, O. P., & Semenov, R. M. (2003). Fault scarps and prehistoric earthquakes in the Tunka fault (southwestern Baikal region). *Russian Geology and Geophysics*, *44*(6), 587–602.
Delouis, B., Déverchère, J., Melnikova, V., Radziminovitch, N., Loncke, L., Larroque, C., et al. (2002). A reappraisal of the source of the 1950 (Mw = 6.9) Mondy earthquake, Siberia, and its relevance to the present-day strain pattern at the southwestern end of the Baikal rift zone. *Terra Nova*, *14*(6), 491–500. https://doi.org/10.1046/j.1365-3121.2002.00445.x
Delvaux, D., Moeys, R., Stapel, G., Melnikov, A., & Ermikov, V. (1995). Paleostress reconstruction and geodynamics of the Baikal region, Central Asia, I, Paleozoic and Mesozoic pre-rift evolution. *Tectonophysics*, *252*(1-4), 61–101. https://doi.org/10.1016/0040-1951(95)00090-9
Déverchère, J., Houdry, F., Diamant, M., Solonenko, N. V., & Solonenko, A. V. (1991). Evidence for seismogenic upper mantle and lower crust in the Baikal rift. *Geophysical Research Letters*, *18*(6), 1099–1102. https://doi.org/10.1029/91GL00851
Déverchère, J., Radziminovich, N., Calais, E., Deschamps, A., Melnikova, V., Petit, C., & Sankov, V. (2000). Seismicity of the Baikal rift and central Mongolia: Seismic potential, search for seismogenic thickness, segmentation and rheological properties of the lithsophere. Seismology in Siberia at the millennium boundary, Novosibirsk Academy Town, Russia, September 27-29, 2000.
Ermikov, V. D. (1994). Mesozoic precursors of the Cenozoic rift structures of Central Asia. *Bulletin du Centre de Recherches Exploration-Production Elf-Aquitaine*, *18*(1), 123–134.
Gao, S., Davis, M., Liu, H., Slack, P., Zorin, Y., Logatchev, N., et al. (1994). Asymmetric upward of the asthenosphere beneath the Baikal rift zone, Siberia. *Journal of Geophysical Research*, *99*(B8), 15,319–15,330. https://doi.org/10.1029/94JB00808
Ionov, D. (2002). Mantle structure and rifting process in the Baikal-Mongolia region: Geophysical data and evidence from xenoliths in volcanic rocks. *Tectonophysics*, *351*(1-2), 41–60. https://doi.org/10.1016/S0040-1951(02)00124-5
Ivanov, A. V., Sankov, V. A., Smekalin, O. P., & Chipizubov, A. V. (2010). Estimation of the recurrence period of strong earthquakes in zone of the Main Sayan and Tunka faults according to the data of radiocarbon dating and statistical analysis. *Seismic Instruments*, *46*(4), 363–371. https://doi.org/10.3103/S0747923910040067
Kondorskaya, N. V., & Shebalin, N. V. (Eds.), 1982. New catalog of strong earthquakes in the USSR from ancient times through 1977. World data center a. Report SE-31, Boulder, USA, (608 pp.).
Lamakin, V. V. (1968). *Neotectonics of the Baikal basin* (in Russian) (247 pp.). Nauka, Moscow.
Larroque, C., Ritz, J. F., Stéphan, J. F., Sankov, V., Arjannikova, A., Calais, E., et al. (2001). Interaction compression-extension à la limite Mongolie–Sibérie: analyse préliminaire des déformations récentes et actuelles dans le bassin de Tunka. *Comptes Rendus. Académie des Sciences*, *332*, 177–184.
Logatchev, N. (1993). History and geodynamics of the Lake Baikal rift in the context of the eastern Siberia rift system: A review. *Bulletin du Centre de Recherches Exploration-Production Elf-Aquitaine*, *17*(2), 353–370.
Logatchev, N., & Zorin, Y. (1987). Evidence and causes of the two-stage development of the Baikal rift. *Tectonophysics*, *143*, 225–234.
Logatchev, N., & Zorin, Y. (1992). Baikal rift zone: Structure and geodynamics. *Tectonophysics*, *208*(1-3), 273–286. https://doi.org/10.1016/0040-1951(92)90349-B
Lukhnev, A. V., Sankov, V. A., Miroshnichenko, A. I., Ashurkov, S. V., & Calais, E. (2010). GPS rotation and strain rates in the Baikal–Mongolia region. *Russian Geology and Geophysics*, *51*(7), 785–793. https://doi.org/10.1016/j.rgg.2010.0%20006
Lunina, O. V., & Gladkov, A. S. (2004). Fault structure of the Tunka rift as a reflection of oblique extension. *Doklady Earth Sciences*, *398*(7), 928–930.
McCalpin, J., & Khromovskikh, V. (1995). Holocene paleosismicity of the Tunka fault (Baikal, Russia). *Tectonics*, *14*(3), 594–605. https://doi.org/10.1029/95TC00837
McCalpin, J. P. (1996). *Paleoseismology* (p. 588). New York: Academic Press.
Melnikov, A. I., Mazukabzov, A. M., Sklyarov, E. V., & Vasiljev, E. P. (1994). Baikal rift basement: Structure and tectonic evolution. *Bulletin du Centre de Recherches Exploration-Production Elf Aquitaine*, *18*(1), 99–122.
Misharina, L., Melnikova, V., & Baljinnyam, I. (1983). Southwestern margin of the Baikal rift zone from the data of earthquake focal mechanisms (in Russian). *Volcanology and Seismology*, *2*, 74–83.
Molnar, P., & Tapponnier, P. (1975). Cenozoic tectonics of Asia. Effects of a continental collision. *Science*, *189*(4201), 419–426. https://doi.org/10.1126/science.189.4201.419
Nataf, H. C., Froidevaux, C., Levrat, J. L., & Rabinowicz, M. (1981). Laboratory convection experiments: The effect of lateral cooling and generation of instabilities in the horizontal layers. *Journal of Geophysical Research*, *86*(B7), 6143–6154. https://doi.org/10.1029/JB086iB07p06143
Nazari, H., Ritz, J.-F., Shafei, A., Ghassemi, A., Salamati, R., Michelot, J.-L., & Massault, M. (2009). Morphological and paleoseismological analyses of the Taleghan fault, Alborz, Iran. *Geophysical Journal International*, *178*(2), 1028–1041. https://doi.org/10.1111/j.1365-246X.2009.04173.x
Parfeevets, A. V., & Sankov, V. A. (2006). Geodynamic conditions of evolution of the Tunka branch in the Baikal rift system. *Geotectonics*, *5*, 377–398.
Radziminovich, N. A., Gileva, N. A., Melnikova, V. I., & Ochkovskaya, M. V. (2013). Seismicity of the Baikal rift system from regional network observations. *Journal of Asian Earth Sciences*, *62*, 146–161. https://doi.org/10.1016/j.jseaes.2012.10.029
Radziminovich, Y. B., & Shchetnikov, A. A. (2013). Historical earthquakes studies in Eastern Siberia: State-of-the-art and plans for future. *Journal of Asian Earth Sciences*, *62*, 134–145. https://doi.org/10.1016/j.jseaes.2012.09.017
Ritz, J.-F., Brown, E. T., Bourlès, D. L., Philip, H., Schlupp, A., Raisbeck, G., et al. (1995). Slip rates along active faults estimated with cosmic ray exposure dates: Application to the Bogd fault, Gobi-Altaï, Mongolia. *Geology*, *23*, 1019–1022.
Ritz, J.-F., Larroque, C., Stéphan, J. F., Sankov, V., Arjannikova, A., Calais, E., Deverchère, J., & Loncke, L. (2000). When compression meets extension: Interaction or competition? The example of the Tunka basin (Western Baikal, Siberia). In Proceedings of the geosciences 2000 (pp. 122). University of Manchester.
Ritz, J.-F., Vassallo, R., Braucher, R., Brown, E., Carretier, S., & Bourlès, D. (2006). Using in situ-produced 10Be to quantify active tectonics in the Gurvan Bogd mountain range (Gobi-Altay, Mongolia). *Geological Society of America Special Papers*, *415*, 87–110.
Rizza, M., Ritz, J.-F., Braucher, R., Vassallo, R., Prentice, C., Mahan, S., et al. (2011). Slip rate and slip magnitudes of past earthquakes along the Bogd left-lateral strike-slip fault (Mongolia). *Geophysical Journal Internaional*, *186*, 897–927.
Rizza, M., Ritz, J.-F., Prentice, C., Braucher, R., Vassallo, R., Larroque, C., et al. (2015). Earthquake geology of the Bolnay Fault (Mongolia). *BSSA*, *105*(1), 72–93. https://doi.org/10.1785/0120140119
Ruzhich, V., Sherman, S., & Tarasevich, S. (1972). Nouvelles données sur les failles inverses dans la partie SW du rift Baïkal. *Doklady Academia Nauk URSS*, *205*, 920–923.

Sankov, V., Miroshnichenko, A., Levi, K., Luknev, A., Melnikov, A., & Delvaux, D. (1997). Cenozoic stress field evolution in the Baikal rift zone. *Bulletin du Centre de recherches Elf Exploration Production*, *21*, 435–455.

Sankov, V. A., Chipizubov, A. V., Lukhnev, A. V., Smekalin, O. P., Miroshnichenko, A. I., Calais, E., & Déverchère, J. (2004). Assessment of a large earthquake risk in the zone of the main Sayan fault using gps geodesy and paleoseismology. *Russian Geology and Geophysics*, *45*(11), 1369–1376.

Sankov, V. A., Lukhnev, A. V., Miroshnitchenko, A. I., Dobrynina, A. A., Ashurkov, S. V., Byzov, L. M., et al. (2014). Contemporary horizontal movements and seismicity of the South Baikal Basin (Baikal rift system). *Izvestiya Physics of the Solid Earth*, *50*(6), 785–794. (original Russian text © in Fizika Zemli, 2014, no. 6, pp. 70–79)

Sengör, A. M. C., Nattal'in, B. A., & Burtman, V. S. (1993). Evolution of the Altaid tectonic collage and Palaeozoic crustal growth in Eurasia. *Nature*, *364*(6435), 299–307. https://doi.org/10.1038/364299a0

Shchetnikov, A. (2016). Morphotectonics of the Tunka rift and its bordering mountains in the Baikal rift system, Russia. *Geomorphology*, *273*, 258–268.

Shebalin, N. V., & Leydecker, G. (1997). *Earthquake catalogue for the former Soviet Union and Bbrders up to 1988* (p. 135). Luxembourg: Office for Official Publications of the European Communities.

Sherman, S. I. (1978). Faults of the Baikal rift zone. *Tectonophysics*, *45*(1), 31–39. https://doi.org/10.1016/0040-1951(78)90221-4

Sherman, S. I., Medvedev, M. E., Ruzhich, V. V., Kiselev, A. I., & Shmotov, A. P. (1973). *Tectonics and volcanism of the southwestern Baikal rift system* (in Russian) (135 pp.). Nauka, Novosibirsk.

Smekalin, O. P. (2008). *The study of the paleoseismic deformations of the Southern Pribaikalie* (p. 101). Moskow: IPE RAS.

Stuiver, M., Reimer, P. J., & Reimer, R. W. (2018). CALIB 7.1 [WWW program] at http://calib.org, accessed 2018-4-30

Tapponnier, P., & Molnar, P. (1977). Active faulting and tectonics in China. *Journal of Geophysical Research*, *82*(20), 2905–2930. https://doi.org/10.1029/JB082i020p02905

Tapponnier, P., & Molnar, P. (1979). Active faulting and cenozoic tectonics of the Tien Shan Mongolia and Baikal regions. *Journal of Geophysical Research*, *84*(B7), 3425–3459. https://doi.org/10.1029/JB084iB07p03425

Tatevossian, R. E., Mokrushina, N. G., Aptekman, J. Y., & Tatevossian, T. N. (2013). On the relevancy of the combination of macroseismic and paleoseismic data. *Seismic Instruments*, *49*(2), 115–138. https://doi.org/10.3103/S0747923913020035

Tiberi, C., Deschamps, A., Déverchère, J., Petit, C., Perrot, J., Appriou, D., et al. (2008). Asthenospheric imprints on the lithosphere in Central Mongolia and Southern Siberia from a joint inversion of gravity and seismology (MOBAL experiment). *Geophysical Journal International*, *175*, 128–1297. https://doi.org/10.1111/j.1365-246X.2008.03947.x

Vergnolle, M., Pollitz, F., & Calais, E. (2003). Constraints on the viscosity of the continental crust and mantle from GPS measurements and postseismic deformation models in western Mongolia. *Journal of Geophysical Research*, *108*(B10), 2502. https://doi.org/10.1029/2002JB002374

Wells, D. L., & Coppersmith, K. J. (1994). Emprical relationships among magnitude, rupture length, rupture area, and surface displacement. *Bulletin of the Seismological Society of America*, *84*, 974–1002.

Zonenshain, L. P., Kusmin, M. I., & Natapov, L.M. (1990). *Plate tectonics and geology of the USSR* (in Russian) (328 pp.). Nedra, Moscow. https://doi.org/10.1029/GD021

Zonenshain, L. P., & Savostin, L. A. (1981). Geodynamics of the Baikal rift zone and plate tectonics of Asia. *Tectonophysics*, *76*(1-2), 1–45. https://doi.org/10.1016/0040-1951(81)90251-1

Zorin, Y. A. (1999). Geodynamics of the western part of the Mongolia-Okhotsk collisional belt, Trans-Baikal region (Russia) and Mongolia. *Tectonophysics*, *306*(1), 33–56. https://doi.org/10.1016/S0040-1951(99)00042-6

Zorin, Y. A., Belichenko, V. G., Turutanov, E. K., Kozhevnikov, V. M., Ruzhentsev, S. V., Dergunov, A. B., et al. (1993). The south Siberia-central Mongolia transect. *Tectonophysics*, *225*(4), 361–378. https://doi.org/10.1016/0040-1951(93)90305-4